energies

MDPI

Article

Multi-Sensor Experimental Investigation of Thermal Runaway and Emissions in a High-Mileage Gasoline Engine Operating at Idle Without Forced Cooling

Iliyan Damyanov [1,*], Durhan Saliev [1], Evgeni Dimitrov [1], Georgi Mladenov [1], Milena Savova-Mratsenkova [1], Hristo Konakchiev [1], Vladimir Hristov [2], Iliyana Naydenova [3], Kalin Dimitrov [4], Rosen Miletiev [4], Lyubomir Laskov [4], Tsvetan Ivanov Valkovski [4], Ivaylo Nachev [4] and Dimitar Asenov [4]

[1] Faculty of Transport, Technical University of Sofia, 8 Kliment Ohridski Blvd, 1756 Sofia, Bulgaria; durhan_saliev@tu-sofia.bg (D.S.); etzd@tu-sofia.bg (E.D.); gmladenov@tu-sofia.bg (G.M.); savova@tu-sofia.bg (M.S.-M.); hkonakchiev@tu-sofia.bg (H.K.)
[2] Faculty of Automatics, Technical University of Sofia, 8 Kliment Ohridski Blvd, 1756 Sofia, Bulgaria; vdhristov@tu-sofia.bg
[3] Faculty of Industrial, Technical University of Sofia, 8 Kliment Ohridski Blvd, 1756 Sofia, Bulgaria; inaydenova@tu-sofia.bg
[4] Faculty of Telecommunications, Technical University of Sofia, 8 Kliment Ohridski Blvd, 1756 Sofia, Bulgaria; kld@tu-sofia.bg (K.D.); miletiev@tu-sofia.bg (R.M.); llaskov@tu-sofia.bg (L.L.); cvalkovski@tu-sofia.bg (T.I.V.); ivaylonachev@tu-sofia.bg (I.N.); dimitar.asenov@tu-sofia.bg (D.A.)
* Correspondence: idamyanov@tu-sofia.bg

Abstract

This study presents a single-case multi-sensor experimental study of thermal loading and emission variation in a high-mileage gasoline engine operating at idle under deliberately impaired cooling until mechanical failure. A production vehicle equipped with a naturally aspirated gasoline engine with a displacement of 1600 cc was operated under relatively steady-state conditions at idle, while gaseous emissions (CO, CO_2, HC, NO_x, and O_2), air–fuel ratio λ, particle number (PN), oil temperature, infrared thermal indicators, and acoustic performance variation were continuously monitored. The results are interpreted primarily in terms of their dependence on the engine oil temperature. They show that despite stable conditions of the air–fuel ratio and an almost constant amount of residual oxygen in the exhaust gases, progressive thermal loading leads to pronounced changes in the behavior of the emissions emitted by the engine during its operation. Hydrocarbon emissions show increased variability and escalation at elevated engine oil temperatures, while nitrogen oxides show a strong temperature-dependent increase, consistent with thermally driven formation mechanisms. The most significant response is observed in the particle number (PN) emissions, which go from low and stable levels to a rapid, multi-step increase in a narrow temperature range preceding mechanical failure. Under the tested cooling impairment scenario, emission behavior was dominated by cumulative thermal stress rather than mixture composition effects. In the investigated case, particle number emissions emerged as a sensitive indicator of system-level thermal instability. The findings provide experimentally documented insight into the system-level progression toward thermal runaway under impaired cooling conditions and its measurable impact on emission behavior in the tested engine.

Keywords: thermal drift; gasoline engine; idling; particle number; exhaust emissions; oil temperature; high-mileage engine; thermal degradation

Academic Editors: Paweł Droździel, Karol F. Abramek and Tomasz Osipowicz

Received: 23 January 2026
Revised: 12 February 2026
Accepted: 21 February 2026
Published: 25 February 2026

1. Introduction

Idle speed is defined in engineering practice as the operating mode of an internal combustion engine in which the torque generated by the combustion process is minimal and sufficient only to overcome internal mechanical friction, for the operation of auxiliary systems (water pump, oil pump, and alternator), and to maintain a minimum stable speed (usually between 600 and 1000). In this state, the throttle valve is almost completely closed, which creates a high vacuum (strong negative pressure) in the intake manifold [1]. It is important to distinguish between "cold idle" and "hot idle". While hot idle represents a relatively stable thermal and lubricating state, prolonged cold idle is the main source of accelerated wear and chemical degradation [2]. Overheating of internal combustion engines remains a critical problem in terms of reliability, emissions, and remaining engine life [3,4]. In most existing studies, engine overheating is investigated under controlled laboratory conditions, on engine test benches, or through numerical and reduced thermal models [5,6]. Experimental studies are rarely carried out until real mechanical failure due to the high risk of irreversible damage to the engine and test infrastructure [7]. Data-transfer capabilities, machine learning (ML), artificial intelligence (AI), and infrared thermography (IRT) are entering as tools for automatic collection and processing of thermographic information in all areas of life [8–14].

Recent studies have shown [15,16] that during prolonged idling, engine oil temperature can increase linearly over time, exceeding temperatures typical of a part-load operation under certain conditions. This is due to a combination of low cooling efficiency, prolonged continuous operation, local hot spots, and additional friction losses that do not decrease proportionally with engine speed.

In high-mileage engines, this effect is even more pronounced due to deposits, poor heat transfer, and degraded lubricating properties of the engine oil [17,18].

Idling is a net waste of energy, as the generated torque is not used for propulsion. Analyses have shown that even under nominal conditions, stationary idling consumes a significant amount of fuel [19,20].

High-mileage engines represent a separate category in terms of their thermal behavior [21,22]. The wear of the piston–cylinder group, valve train, and bearings leads to increased friction, increased heat generation, greater gas penetration into the crankcase (blow-by), and poor temperature distribution in the engine.

Data from the literature show [23,24] that in engines with mileage exceeding 300,000 km, even relatively small deviations in the cooling mode can lead to a sharp increase in the temperatures of the oil and metal assemblies. This effect is amplified when using high-mileage engine oil, in which the additive package is partially or completely depleted.

The valve train area is particularly sensitive [25–27], where contact loads are high and cooling is mainly limited to the oil flow. With prolonged thermal exposure, this can lead to accelerated wear or local damage, which ultimately also affects the acoustic signature of the engine.

Engine oil simultaneously performs lubrication, cooling, and cleaning functions [28,29]. When the temperature rises above certain threshold values, processes of thermo-oxidative decomposition, loss of viscosity, destruction of antifriction additives, and formation of solid particles and deposits begin.

A number of experimental studies have shown that at temperatures above 110–120 °C, the rate of oil degradation increases non-linearly [30,31]. This means that even short periods of overheating can have a long-lasting effect on the lubricating properties [32].

In the context of an engine with high mileage, used oil, and limited cooling, conditions are created for thermo-tribological runaway, in which increased friction leads to even greater heat generation, which in turn accelerates the destruction of the oil film [33,34].

https://doi.org/10.3390/en19051137

Exhaust emissions are often considered an indicator of the quality of the combustion process. Under normal conditions, the ratios between CO, CO_2, HC, NO_x, and O_2 are relatively stable at idle; however, under thermal overload, these relationships are disrupted [35,36].

The increased temperature in the combustion chamber and exhaust system leads to the following processes:

- Increased formation of NO_x due to the thermal mechanism;
- Changes in the composition of the residual oxygen;
- Instability of the lambda control;
- Potential increase in hydrocarbons due to poor combustion and oil burning.

The catalytic converter under such conditions may operate outside its optimal temperature range, which further complicates the interpretation of the measured emissions [37–39].

The acoustic signal of a running engine contains information about its mechanical condition. An increase in noise, the appearance of pulse peaks, or a change in the frequency spectrum often precede mechanical failures [40].

It is assumed in the literature [41–43] that the increase in high-frequency noise components may be associated with deterioration of lubrication, increased contact loads, local metal-to-metal friction, or early stages of damage.

Combining acoustic data with thermal and emission measurements allows for a much more reliable interpretation of the processes occurring in the engine, especially in experiments leading to failure [44,45].

Thermal runaway in internal combustion engines is characterized by a positive feedback loop between temperature, friction, and lubrication degradation [46]. An increase in temperature leads to a decrease in oil viscosity, which in turn increases the contact friction between moving parts [47]. This generates additional heat, accelerating the process until local seizure and complete mechanical failure occur [48].

While thermal runaway mechanisms have been conceptually described in simulation-based studies and accelerated bench tests [49], the progressive development of the phenomenon under real vehicle conditions—culminating in actual mechanical seizure—remains insufficiently documented. In particular, experimental datasets capturing the full transition from thermal imbalance to irreversible engine blocking in production vehicles are scarce due to the destructive and non-repeatable nature of such tests [50].

In real-world conditions, this process often runs uncontrollably and leads to mechanical failure (seizure), especially in engines with high mileage and an already compromised lubrication system [51]. Recent publications confirm that lubricating oil can be a measurable source of particle number (PN) emissions in gasoline engines, particularly under conditions that promote elevated oil temperature, vaporization, and transport of oil-derived material into the combustion chamber [52,53]. Experimental studies have shown that fuel–lubricant interactions and thermally induced changes in lubricant volatility can alter PN behavior, even when the air–fuel ratio remains nominally stoichiometric [54,55]. Reviews of lubricant-related particle formation further emphasize that oil consumption pathways, additive chemistry, and cumulative thermal exposure affect both the volatile and nonvolatile fractions of the particles [56,57]. At high component temperatures, accelerated degradation and evaporation of the oil film can contribute to a multi-step escalation of PN, especially near the limits of thermal stability [58]. In this context, the sharp increase in PN observed with progressive increases in oil temperature is consistent with thermally driven mechanisms related to the lubricant, although a composite analysis would be required to definitively determine the source.

The aim of this study is to experimentally analyze the development of thermal runaway in a gasoline engine with high mileage, operating for a long time at idle without forced cooling until the occurrence of complete mechanical failure (engine blocking). The analysis in this publication is focused primarily on the change in gas emissions, the number of particles in the exhaust gases, and the interrelationships between these parameters from increasing temperature loads to operation in conditions of loss of thermal equilibrium.

2. Materials and Methods

The object under study is a Fiat Marea (Fiat Automobiles S.p.A., Turin, Italy) passenger car, manufactured in 1997, equipped with a gasoline engine with a displacement of 1600 cc and a rated power of 74 kW. The engine has a classic architecture for the period, naturally aspirated and with multi-point fuel injection.

The total mileage of the engine at the time of the experiment was 356,724 km, with most of this mileage being realized when operating on LPG. The engine oil had a mileage of 26,724 km, without a change performed immediately before the experiment, which allows the study of real, degraded lubricating oil in conditions close to the real operation of a car with high mileage.

The experiment started at approximately 14:30 local time under stable ambient conditions. The ambient air temperature was between 18 and 20 °C. During the test, the wind was moderate north–northwest. The relative humidity was approximately 55%, with a dew point of 10 °C. The sky was characterized by variable cloudiness. The atmospheric pressure during the experiment was 760 mmHg (953 hPa), and the environmental conditions remained stable throughout the experiment and did not show any sudden changes.

The experiment was conducted in stationary idling mode, with the engine speed maintained in the range of 850–860 min^{-1}. The engine was running on gasoline during the experiment. In order to create controlled conditions of increased thermal load, the cooling system fan was dismantled, which eliminated forced air cooling of the radiator.

In this way, the engine is cooled only by:

- Natural convection;
- Heat exchange with the environment;
- Circulation of the coolant until it boils.

The total duration of the experiment was approximately 70 min, at the end of which the engine reached a state of thermal runaway and mechanical blocking (seizure). Figure 1 shows a scheme of the experimental setup of the study. All images used in this publication were made by the authors during the experimental setup and have no external source.

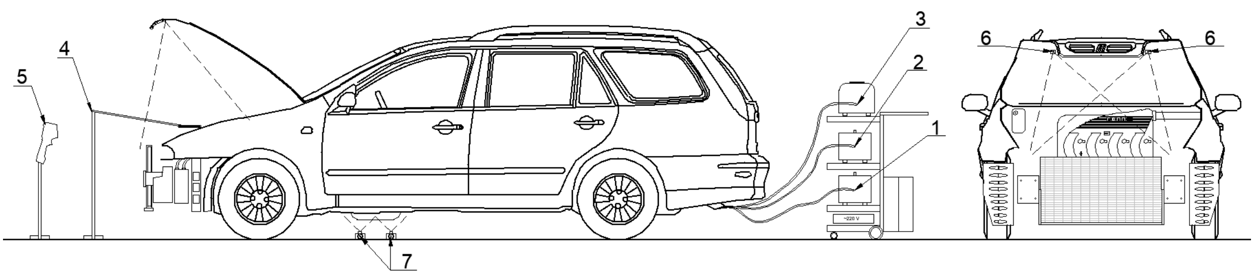

Figure 1. Scheme of the experimental setup of the study: 1—gas analyzer, Texa Gasbox (TEXA S.p.A., Monastier di Treviso, Italy); 2—gas analyzer, Brain Bee AG-200 (Brain Bee S.p.A., Parma, Italy); 3—diffusion charging (DC) particle number concentration (PNC) (TEXA S.p.A., Monastier di Treviso, Italy); 4—microphone, USB Noise Meter (Spl-Lab, The Woodlands, TX, USA); 5—thermal imaging camera, RayThink RM200F (Raythink Technology Co., Ltd., Shenzhen, China); 6 and 7—thermal imaging camera, Melexis MLX90640 (Melexis NV, Tessenderlo, Belgium).

For the purposes of the study, a multi-sensor measurement system was built, allowing simultaneous monitoring of the thermal, emission, acoustic, and mechanical behavior of the engine.

During the experiment, two independent five-component gas analyzers were used (Figure 2: (a) Brain Bee AGS-200 [59]; (b) Texa Gasbox [60]), simultaneously measuring carbon monoxide (CO), hydrocarbons (HC), carbon dioxide (CO_2), nitrogen oxides (NO_x), and oxygen (O_2), while additionally recording the air–fuel ratio (λ), engine speed (rpm), and engine oil temperature (°C). This approach provides a complete description of the combustion products and the operating state of the engine under thermal instability conditions.

(**a**) (**b**)

Figure 2. Gas analyzers: (**a**) Brain Bee AGS-200; (**b**) Texa Gasbox.

The use of two gas analyzers allows independent registration of the same parameters under identical operating conditions, which is especially important in long-term experiments leading to mechanical failure, when the composition of the exhaust gases and the temperature conditions can change rapidly and non-linearly. The comparison between the two datasets shows very good quantitative agreement, with the deviations between the measurements remaining minimal throughout the experiment.

For the purposes of the subsequent analysis, the data from the two gas analyzers were used together. The tabular and graphical dependencies presented in this work are built on the basis of the combined information, with the consistency between the two measurement channels serving as an additional check for the reliability of the observed trends in engine emission behavior.

To measure the particle number concentration (PNC), the Texa device NP 01 was used, connected to the exhaust system, with the following technical characteristics: diffusion charge (DC) technology; measuring range 5000–5,000,000 cm^{-3}; particle size 23–200 nm; resolution 1000 cm^{-3}; and error (absolute) 25,000 cm^{-3}—indicating the absolute error of the measuring instrument (Figure 3). This device was developed in accordance with the technical specifications required by the Dutch regulation N-PTI [61] and the German PTB-A 12.16 [62]. The parameter is particularly important at high temperatures and oil degradation, when particles originating from oil, carbon deposits, and metal wear may appear in the exhaust gases.

Figure 3. Diffusion charging (DC) particle number concentration (PNC).

The thermal behavior of the engine and cooling system was monitored through several independent thermographic channels (Figure 4):

1. Handheld thermal imaging camera RayThink RM200F—equipped with a self-developed uncooled infrared detector with dimensions 256 × 192 I 20 °C~+550 °C, wide measurement range for monitoring more temperature targets [63], located frontally to the engine and radiator, used for:
   - Assessment of the engine temperature field;
   - Monitoring of the radiator and cooling dynamics.
2. To monitor the overall temperature of the engine compartment from different positions, two multi-pixel infrared (IR) sensors were installed, model MLX90640 Thermal Camera Breakout-Wide angle (110) [64], which offers a resolution of 32 × 24 pixels and a field of view of 110° × 75°. Two compact thermal cameras were mounted on the front hood and aimed at the engine from above to:
   - Track local temperature zones;
   - Record temperature gradients and hot spots.

(**a**) (**b**)

Figure 4. Thermal imaging: (**a**) RayThink RM200F handheld thermal imaging camera; (**b**) multi-pixel infrared (IR) sensor, model MLX90640.

It is important to note that the exhaust manifold is not directly visible to the thermal cameras due to its structural location at the rear of the engine. Therefore, temperature estimates in this area are treated with caution and are not used as a direct measure of the temperature of the gases in the cylinder.

The catalytic converter was monitored by two multi-pixel infrared (IR) sensors, model MLX90640 Thermal Camera Breakout-Standard (55°) [65]—which offers a resolution of 32 × 24 pixels and a field of view of 55° × 35° (Figure 5)—located before and after the catalyst. Infrared sensors mounted on telescopic supports were positioned at fixed distances from the catalytic converter housing to enable continuous non-contact surface-temperature measurement during the experiment.

Figure 5. Arrangement of infrared sensors for upstream and downstream catalytic-converter-housing temperature monitoring.

It should be emphasized that the catalyst is located in an external thermal jacket, which means that the measured temperature represents a surface temperature, and not a direct temperature, of the active catalytic zone. This was taken into account when interpreting the results.

For the purpose of synchronization during data processing, all measured parameters were referenced to a common time axis, representing the real duration of the experiment. The experiment was videotaped to further specify time markers, which allows a direct connection between the numerical data and the visual information from the experiment.

It should be emphasized that the present work represents a single-case experimental investigation conducted on one high-mileage production engine under a deliberately induced cooling-impairment scenario. The test condition does not represent standard idling operation in a healthy vehicle; instead, it represents impaired heat rejection due to loss of forced convection at the radiator, serving as a controlled fault scenario to study the progression toward thermal runaway and its emission consequences. The objective is not to generalize statistically representative behavior, but to provide a detailed, time-resolved characterization of thermal and emission evolution under progressive heat-rejection loss.

2.1. Measurement Uncertainty

The gas analyzer and particle counter were operated within manufacturer-specified accuracy limits. Typical measurement uncertainties were ±(2–3)% of the reading for gaseous species and within ±(3–5)% for the particle number concentration under steady-state conditions. Infrared surface-temperature measurements are subject to emissivity-related uncertainty and are estimated to be within ±2 °C for the applied emissivity settings.

Since the present study focuses on trend evolution and order-of-magnitude transitions rather than absolute calibration-based quantification, the reported thermal and emission transitions exceed the expected measurement uncertainty by a substantial margin.

2.2. Safety Considerations

The experiment was conducted in a controlled outdoor/ventilated area with fire safety equipment available and continuous operator supervision. The test was terminated only after documented loss of functional operation; all measurements were performed without personnel exposure to exhaust. Spilled coolant was contained and disposed of according to local environmental procedures. The study design intentionally induced thermal overload; therefore, replication should be performed only under appropriate risk management and safety protocols.

https://doi.org/10.3390/en19051137

3. Results

3.1. Operating Conditions and Temporal Reference of the Experiment

The experiment was designed to reproduce a controlled loss-of-heat-rejection scenario (forced-air cooling impairment), representative of fault conditions such as fan failure, reduced airflow, or cooling system malfunction. The goal was not to emulate normal idling, but to observe the coupled thermal and emission response during progressive thermal overload until the onset of runaway. During the test, the engine speed remained within the nominal idling range (approximately 850–860 rpm), with only minor fluctuations inherent to idling. No intentional changes to the engine control parameters were applied during the experiment.

The air–fuel ratio remained close to stoichiometric for most of the test duration, indicating stable mixture control despite progressive thermal loading. Fuel delivery was maintained only with gasoline after a long period of vehicle inactivity and with old operating fluids. Figure 6 presents the time evolution of the engine speed and air–fuel ratio during the experiment.

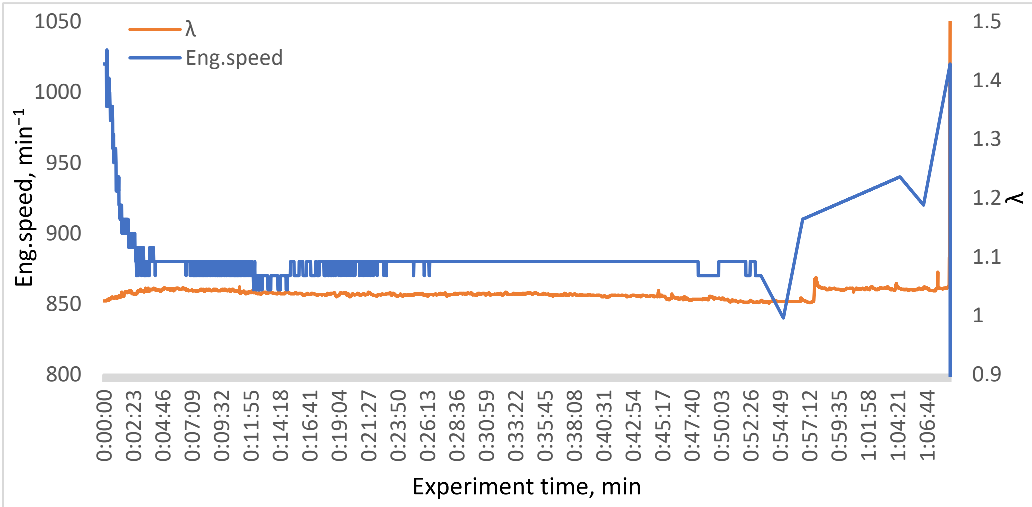

Figure 6. Engine speed vs. air ratio (λ).

All measurement systems were time-synchronized and referenced to a common experimental timeline. The experiment continued without interruption until complete mechanical blockage occurred, which determined the temporal endpoint of the results presented in this section.

The lack of significant variations in engine speed and λ establishes a consistent operating baseline. Therefore, the observed thermal escalation and subsequent emission changes discussed in the following sections cannot be attributed to changes in engine control parameters, but rather to the progressive accumulation of thermal load resulting from the lack of forced cooling. The following analysis focuses on the evolution of the engine thermal state and its role as a primary driver of emission changes during idling without forced cooling.

3.2. Thermal State of the Engine as a Driver for Emission Changes

This section examines the evolution of the engine thermal state during the experiment and its role as a leading factor in the observed emission changes. The analysis is based on synchronized measurements of oil temperature, surface temperatures from the infrared camera, and the behavior of the cooling system, with all of the data presented in a time sequence.

3.2.1. Engine Overheating Under Idling Without Forced Cooling

To provide a comprehensive thermal timeline, three time-resolved temperature indicators are presented on the same experimental time axis: engine oil temperature (Figure 7), maximum engine surface temperature from infrared thermography, and cooling radiator surface temperature from infrared thermography. These signals represent different physical layers of the thermal system (integrative bulk state, local surface maxima, and heat-rejection response). They are shown as separate figures to preserve readability and to avoid over-plotting effects arising from different sampling characteristics and noise levels. Representative thermographic images of the engine at characteristic stages are presented separately (Figure 8) to illustrate spatial temperature distribution, while the interpretation in Sections 3.2.1 and 3.2.2 is performed in a coupled manner.

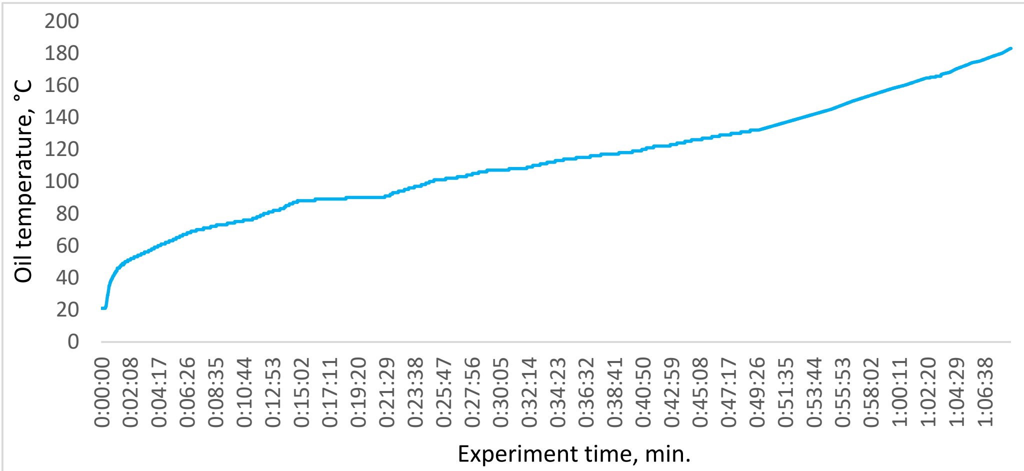

Figure 7. Oil temperature vs. time.

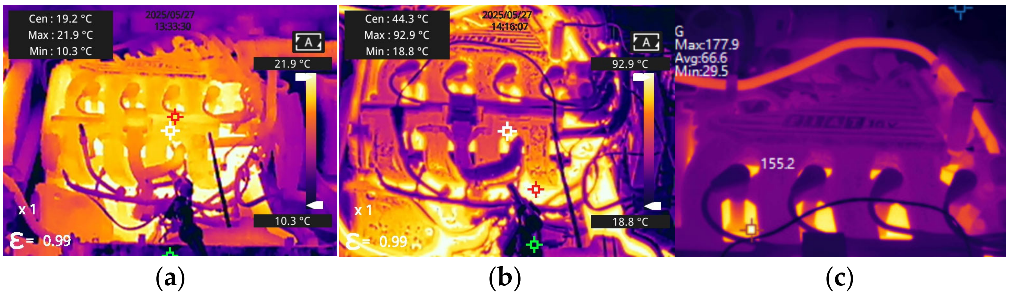

Figure 8. Infrared thermal images of the engine recorded at three characteristic stages of the experiment: (**a**) at the beginning; (**b**) in the middle; (**c**) at the final stage. Colored squares indicate the selected measurement regions used for extracting maximum surface temperature values.

Figure 7 shows the engine oil temperature as a function of time. After the engine was started, the oil temperature increased continuously throughout the experiment without reaching a stable plateau. The temperature increase continued despite no changes in the engine speed or air–fuel ratio, indicating a progressive accumulation of heat energy in the engine. The oil temperature increased from approximately 20 °C at engine start to 179 °C at the moment of mechanical blockage, without reaching any stationary plateau during the entire 70 min experiment.

The infrared surface temperature shows a faster response to progressive thermal loading, reflecting local heat accumulation and reduced heat dissipation at the engine's structural level. In contrast, the oil temperature increases more gradually, representing the integrated thermal state of the engine and the cumulative thermal load experienced by the lubrication system.

Figure 8 presents infrared thermographic images of the engine recorded at three characteristic stages of the experiment: (a) at the beginning of operation at low thermal load; (b) during intermediate stable thermal development; (c) at the final stage, corresponding to the highest thermal load. The images illustrate the progressive increase in surface temperatures and the increasing spatial inhomogeneity of the thermal field as the experiment progresses.

Figure 9 presents the time evolution of the maximum engine surface temperature measured by infrared thermography during idling without forced cooling. From the beginning of the experiment, the engine temperature increased continuously without reaching a stable plateau. In the early phase, the temperature increase was moderate and consistent with the normal warm-up behavior under idling conditions.

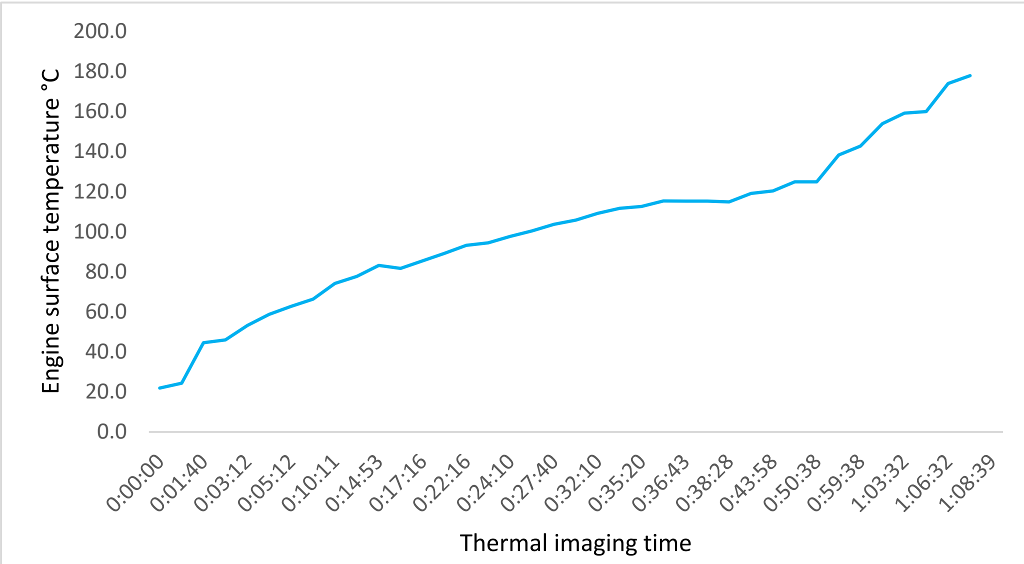

Figure 9. Maximum engine surface temperature (IR) vs. time.

The time derivative of the engine surface temperature calculated by Equation (1) is shown in Figure 10, revealing a progressive increase in the heating rate during the experiment. During the initial phase, *dT/dt* remains relatively low, which corresponds to the normal heating of the engine structure.

$$\left(\frac{dT}{dt}\right)_i = \left(\frac{T_{i+1} - T_i}{t_{i+1} - t_i}\right) \quad (1)$$

where

T_{ii}—maximum engine surface temperature;

t_i—time of the thermographic image.

In this work, the initial phase refers to the warm-up and early stabilization period, the intermediate phase refers to the stable interval before the coolant boils, and the final phase refers to the post-boiling regime, where heat rejection declines and thermal runaway develops.

Figure 10 shows the time derivative of the maximum engine surface temperature calculated according to Equation (1). In the initial phase of the experiment, the heating rate decreases compared to the first minutes after engine start, which corresponds to the normal transient warm-up behavior and partial stabilization of heat distribution within the engine structure. During the intermediate phase, dT/dt fluctuates within a relatively narrow range without pronounced acceleration, indicating a temporarily quasi-balanced thermal state under idling. After approximately 50 min, a sustained increase in dT/dt is observed, indicating a loss of thermal quasi-equilibrium and reduced effective heat-rejection capacity. This acceleration reflects the deterioration of heat-rejection capacity and marks the transition toward the thermally unstable behavior preceding mechanical failure.

The simultaneous increases in surface and oil temperatures indicate a continuous deterioration of thermal equilibrium, providing the thermal framework for the emission evolution analyzed in the next section. Therefore, oil temperature is used as the main reference parameter for correlating gaseous emissions and particle number with the engine thermal state.

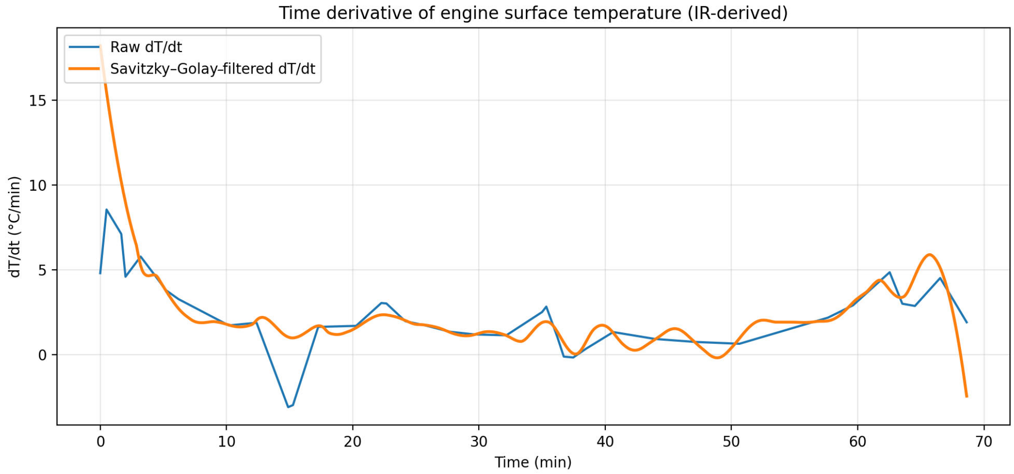

Figure 10. Time derivative of the engine surface temperature (dT/dt) derived from infrared measurements.

3.2.2. Cooling System Response and Loss-of-Heat-Rejection Capacity

Figure 11 presents a graph of infrared thermographic images of the car's cooling radiator, recorded in three characteristic stages of the experiment: (a) under stable temperature conditions (operating temperature); (b) during the boiling temperature; (c) in the final stage after cooling system failure.

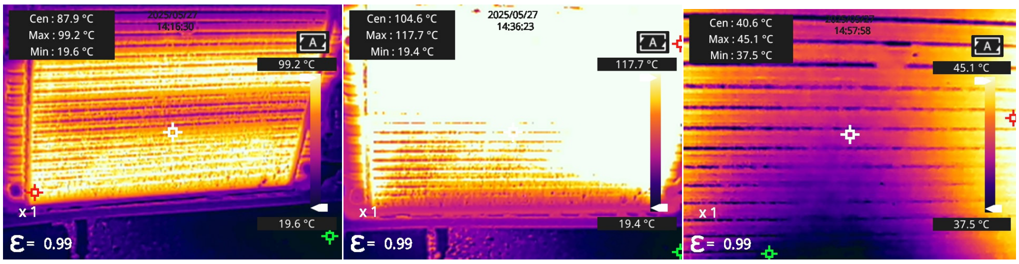

(**a**) (**b**) (**c**)

Figure 11. Infrared thermal images of the cooling radiator surface temperature: (**a**) operating temperature; (**b**) boiling temperature; (**c**) at the final stage, colored squares indicate the selected measurement regions used for extracting maximum surface temperature values.

The response of the cooling system was assessed by infrared measurements of the radiator surface temperature. At a cooling system operating pressure of approximately 0.17 MPa, a maximum radiator surface temperature of approximately 115–117 °C was reached, which coincided with the onset of boiling of the coolant and its subsequent expulsion from the expansion tank (Figure 12). This event occurred at approximately 36:10–36:15 min, marking the transition from controlled to uncontrolled thermal accumulation, after which a pronounced decrease in the radiator surface temperature was observed, despite the continued increase in engine and oil surface temperatures. This behavior indicates a sudden loss of effective heat transfer in the cooling circuit caused by a phase change of the coolant, vapor formation, and partial or complete interruption of the fluid flow through the radiator.

(**a**) (**b**) (**c**)

Figure 12. Moment of cooling system failure: (**a**) real picture; (**b**) thermal picture; (**c**) cooling radiator, colored squares indicate the selected measurement regions used for extracting maximum surface temperature values.

Figure 13 presents a graph of the maximum surface temperature of the cooling radiator over time, measured by infrared thermography during idling without forced cooling. The successive thermographic frames around the moment of coolant discharge show both high temperatures in the expansion tank area and the subsequent temperature state of the cooling radiator, immediately before a drop in its temperature, according to the trend in Figure 13 (radiator surface temperature vs. time).

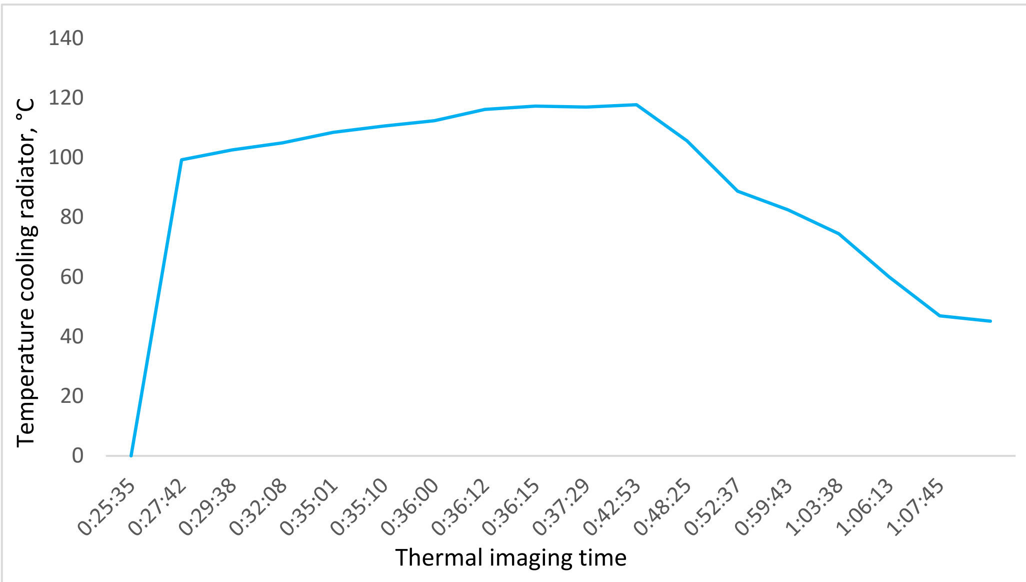

Figure 13. Cooling radiator surface temperature (IR) vs. time.

After the loss of coolant, the radiator temperature progressively drops to levels close to ambient, confirming that the radiator is no longer thermally coupled to the engine as an active heat exchanger. At this stage, the cooling system ceases to provide significant heat removal and the engine enters a regime dominated by uncontrolled heat accumulation. The divergence between engine surface temperature and radiator surface temperature constitutes direct experimental evidence of the loss of thermal coupling between the engine block and the cooling circuit.

3.2.3. Thermal Behavior of the Catalytic Converter Housing Under Progressive Engine Overheating

The thermographic analysis of the external surface of the car's catalytic converter is presented, starting at 15:30 min from the start of the experiment. This moment corresponds to the achieved stable operating thermal regime of the engine, characterized by an engine oil temperature of about 88 °C, which is an indicator of an established steady state at idle. Thus, the analysis is focused on the phase in which the thermal processes in the exhaust system are determined by a steadily generated heat flow, and not by transient effects associated with a cold start.

Figure 14 presents the temperature of the external surface of the catalytic converter measured before and after the catalyst using infrared thermography, starting from a stabilized operating state of the engine (oil temperature ≈ 88 °C). The observed increase in the external temperature of the catalyst, accompanied by the preservation of a clearly pronounced temperature gradient between the inlet and outlet parts, indicates a progressive increase in the heat flow through the exhaust system. The change in this gradient over time reflects changes in the heat balance of the catalyst under conditions of increasing thermal load on the engine and limited heat removal to the environment.

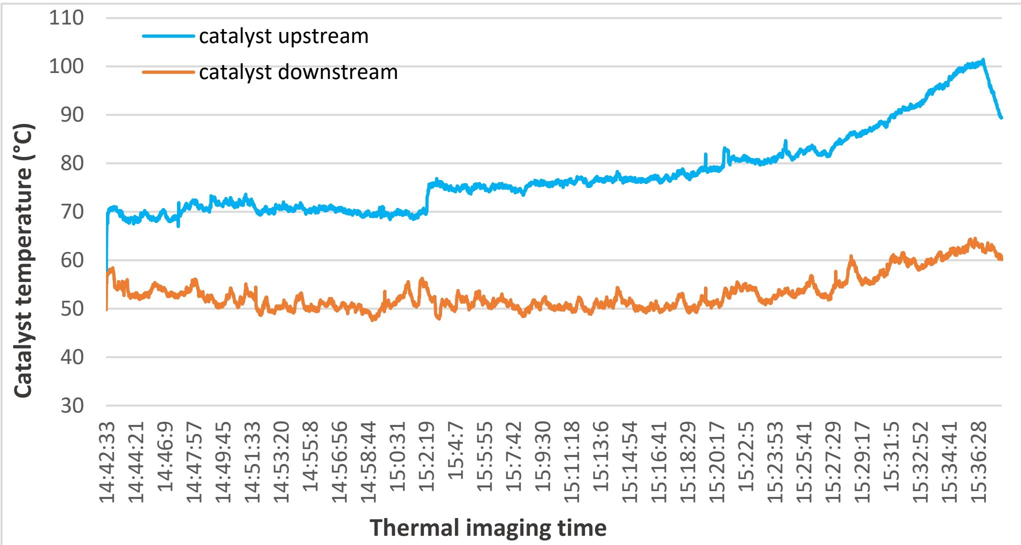

Figure 14. External surface temperature of the catalytic converter measured upstream and downstream (IR) vs. time.

The measurements were performed on the external thermal jacket of the catalyst, and not by means of integrated temperature sensors in the active element. This approach was chosen in order to non-intrusively monitor the thermal load of the exhaust system, without changing the gas flow, local heat exchange, or catalytic conditions. Therefore, the obtained temperatures are not interpreted as the operating temperature of the catalytic element, but as an indicator of the heat release of the catalyst to the environment and the spatial distribution of the heat flow along its length.

Simultaneous thermographic monitoring of the upstream and downstream parts of the catalyst allows for analysis of the temperature difference along the length of the housing, which reflects both the intensity of the heat flow from the exhaust gases and the change in heat transfer with increasing thermal load. The observed systematic decrease in temperature from inlet to outlet, as well as the evolution of this difference over time, indicates a change in the heat balance of the exhaust system under conditions of progressive engine overheating.

The temperature conditions documented in Section 3.3 provide the reference framework for interpreting the emissions of CO, CO, O_2, HC, NO_x, and particle number.

3.3. Gaseous Emission Evolution Under Progressive Thermal Loading

The change in the values of the considered components in the exhaust gases is analyzed depending on the change in the thermal load of the internal combustion engine. The temperature of the engine oil is taken as the main thermal reference indicator. The changes in the operation process are evaluated when the engine is idling with a relatively constant crankshaft rotation frequency (between 850 and 860 rpm). Under these conditions, the change in the values of the evaluated components is also taken into account, including the air ratio of the fuel–air mixture, which is stoichiometric during the experiment, as can be seen from the graph shown in Figure 6.

3.3.1. Hydrocarbons (HC) and Carbon Monoxide (CO) Analysis

Figures 15 and 16 present, respectively, the variations in HC and CO emissions as a function of engine oil temperature. The individual components allow their clear identification and subsequent analysis, given their influence on the engine thermal load and the mechanism of their formation.

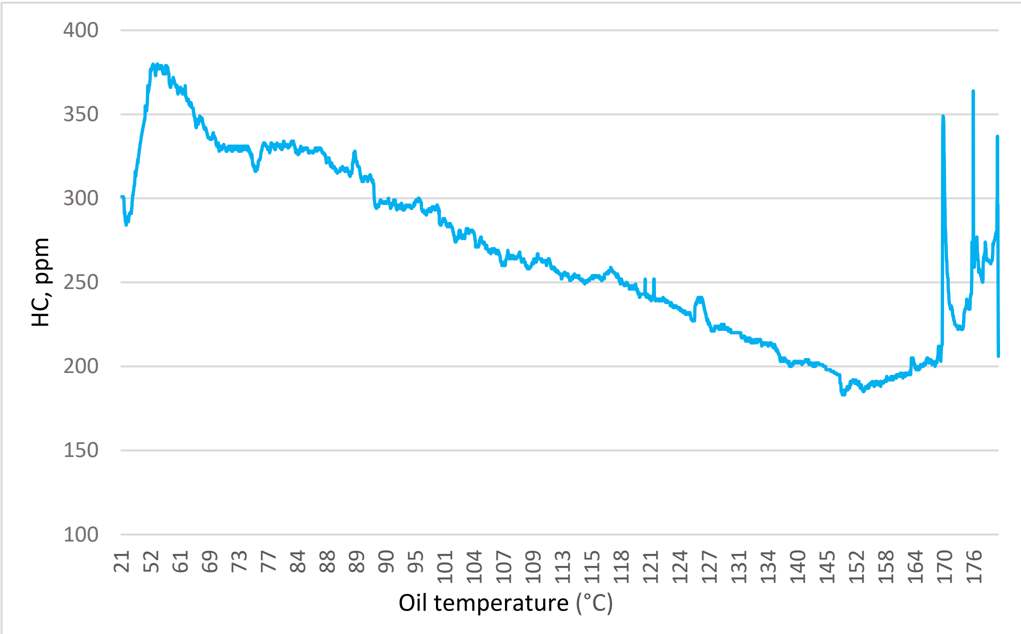

Figure 15. Total hydrocarbon (HC) concentration as a function of engine oil.

The hydrocarbon emissions released during the experiment show non-monotonic behavior with increasing oil temperature. After an initial decrease in the hydrocarbon concentration at oil temperatures of about 20 °C, a clear increase is observed, reaching the highest value of 380 ppm during the experiment, obtained at an engine oil temperature of 54 °C. This behavior is normal during cold-start operation of the engine, which includes low temperatures of the cylinder walls and fuel and the inability, at this initial moment, to reach the temperature required for the oxidation process, causing incomplete fuel combustion. In these cases, other causes are also possible, such as evaporation of lubricants and degradation of the oil film formed during normal operation of the lubrication system.

After the initial increase in hydrocarbons, their gradual decrease follows, which is also expressed after reaching the operating temperature of the engine oil and the continued increase in its temperature. The lowest value of the emitted hydrocarbons of 183 ppm is achieved at an engine oil temperature of 149 °C, which shows that the increase in the temperature of the engine oil, accompanied by the overall increase in its thermal load, has a beneficial effect on the complete combustion of the fuel. An important factor in this case is the unchanged stoichiometry of the fuel–air mixture.

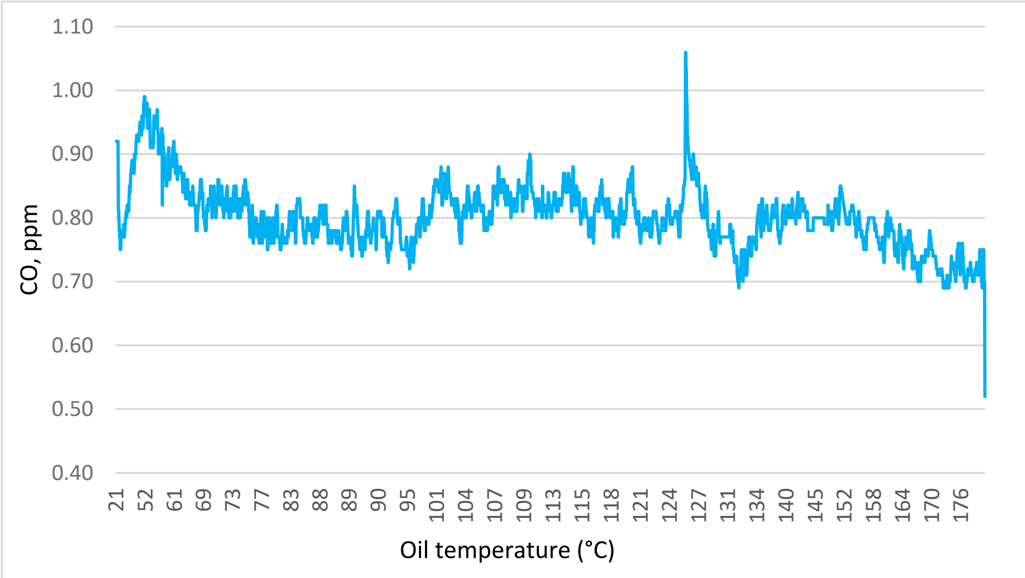

Figure 16. Carbon monoxide (CO) concentration as a function of engine oil temperature during idling without forced cooling.

This is followed by a smooth increase in hydrocarbons and minor fluctuations of around 200 ppm in the engine oil temperature range from 149 °C to 169 °C. The results show that 10 s after reaching this temperature, there is a sharp increase in emitted hydrocarbons, reaching a value of around 343 ppm, followed by sharp fluctuations with values from 222 ppm to 364 ppm in the remaining time until the engine stops working when the moment of its blocking is reached. It is important to note that this occurs in air ratio conditions, which show values above the upper stoichiometric mixture limit of 1.03. Each of the values in the range of fluctuations of the emitted hydrocarbons at the oil temperatures of 169 °C to 179 °C is determined at an air ratio of about 1.04, which changes smoothly until the last 5 s of the experiment, in which the air ratio increases sharply, and in its penultimate value is 1.77, and in the last value is 4.07. However, the value of the hydrocarbons remains below about 280 ppm, and after an increase of 337 ppm 5 s before the end of the experiment, in its last value, the emitted hydrocarbons are 208 ppm.

In contrast, the CO emissions remain in a relatively narrow concentration range during the course of the experiment. Although there are short-term fluctuations, no systematic uncontrolled behavior is observed.

A significant increase in CO values up to 0.99 ppm is observed at the beginning of the experiment at low engine oil temperatures in the range from 21 °C to 58 °C. This is followed by a gradual decrease in the values, which fluctuate slightly around 0.8 ppm during the experiment. It can be seen that there is an extreme increase in the emitted values of this component up to 1.06 ppm, which occurs at an engine oil temperature of 126 °C. This is followed by a gradual decrease in the values to 0.69 ppm at 132 °C of the engine oil, the lowest value of which (excluding the last recorded value of 0.52 ppm at the end of the experiment, since it is not considered relevant given the way in which carbon oxides are formed) is also achieved at an engine oil temperature of 178 °C.

The maintenance of relatively uniform carbon monoxide values during the experiment can be assumed to be due to the operation of the catalytic converter. This is also confirmed by the values of the measured carbon dioxide emissions (Figure 17). The trend in them is inversely proportional to the changes in carbon monoxide values, which indicates normal operation of the oxidation function of the three-component catalytic converter.

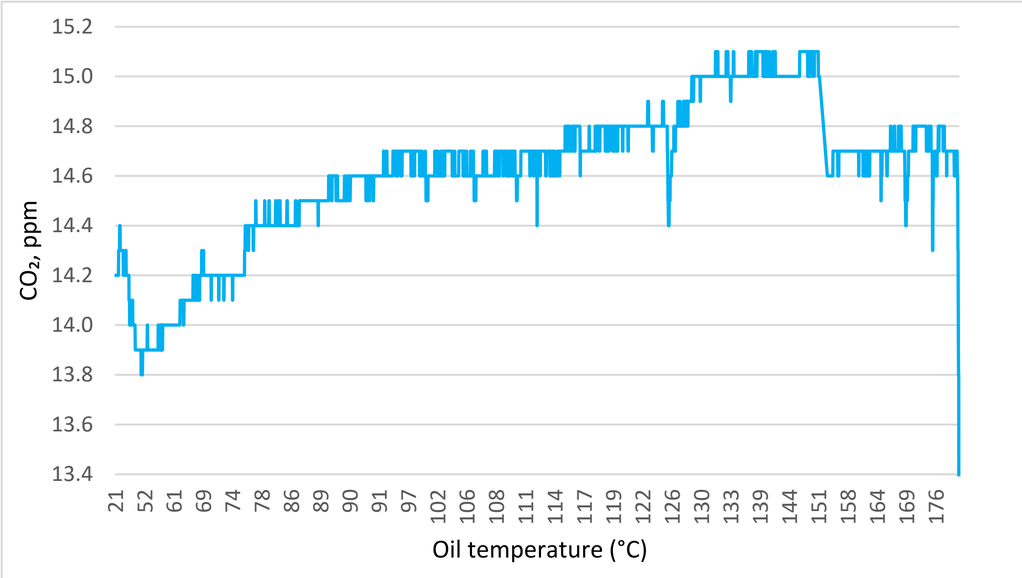

Figure 17. Carbon dioxide (CO_2) concentration as a function of engine oil temperature.

3.3.2. Nitrogen Oxides (NO_x) Evolution and Oxygen (O_2) Availability

While CO and HC mainly reflect the efficiency of the combustion process, the oxidation process in the combustion chamber and the processes related to hydrocarbons, the formation of nitrogen oxides is regulated by different mechanisms, strongly influenced by the temperature and pressure values in the cylinder of the internal combustion engine. In order to distinguish the thermally induced formation of NO_x from the effects related to the combustion of the fuel–air mixture, the presence of residual oxygen in the exhaust gases was first investigated as a reference parameter for the formation of nitrogen oxides.

Figure 18 presents the variation in the oxygen concentration in the exhaust gases as a function of the engine oil temperature. During most of the experiment, O_2 remained almost constant, with values between 1.5% and 2.0%, which indicates stable conditions of the air–fuel ratio, despite the continuous increase in the thermal load of the engine. This behavior confirms that the mixture preparation and its stoichiometric state remain relatively stationary and do not undergo systematic changes during the process of conducting the experiment.

The results show that in the range between 127 °C and 152 °C of the engine oil temperature, a gradual decrease in the residual oxygen values in the exhaust gases is observed, which corresponds to an increase in the carbon dioxide values and a relative decrease in the carbon monoxide values. This indicates an improvement in the combustion process, which contributes to the desired processes of reducing the released components that are harmful to humans in the exhaust gases of the car.

The lack of a progressive decrease in the oxygen concentration suggests that the observed changes in emissions cannot be attributed to the effects of oxygen depletion or enrichment. The sharp increase in O_2 observed in the last stage of the experiment coincides with the onset of unstable combustion and engine blocking, which reflects incomplete oxidation and the presence of unreacted oxygen rather than a controlled change in the formation of the fuel–air mixture.

https://doi.org/10.3390/en19051137

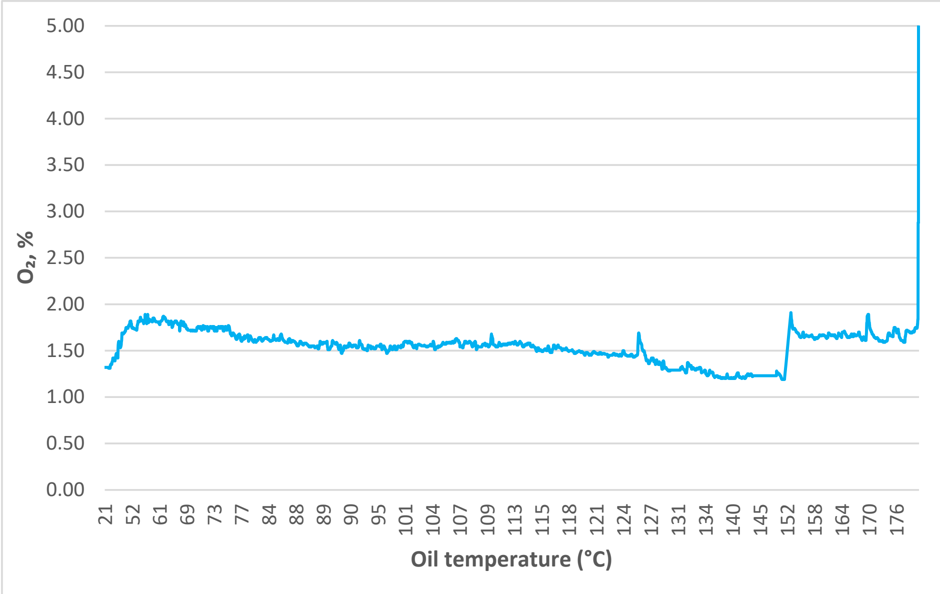

Figure 18. Oxygen concentration (O_2) as a function of engine oil temperature.

Figure 19 shows the corresponding variation in the nitrogen oxide concentration as a function of engine oil temperature. After an initial stabilization phase during engine warm-up, nitrogen oxides gradually and continuously increase with increasing engine oil temperature. Quantitatively, NO_x concentrations increased from approximately 80–90 ppm during the stabilized regime to 800–1000 ppm in the high-temperature range above 150 °C, representing a sustained temperature-dependent increase rather than a mixture-driven fluctuation. This trend becomes significantly steeper in the high-temperature regime preceding engine stall, indicating a transition from a linear increase to an accelerated formation of NO_x. Considering the stable oxygen concentration observed in the relevant temperature ranges, the increase in NO_x can be attributed primarily to thermally driven formation mechanisms. The increased combustion temperatures, increased thermal stress, and presumably increased cylinder pressure of the internal combustion engine under idling conditions without forced cooling contribute significantly to the thermal formation of NO_x. The pronounced rise and increased fluctuations observed towards the end of the experiment are consistent with the loss of temperature control, local overheating, and deterioration of the combustion process.

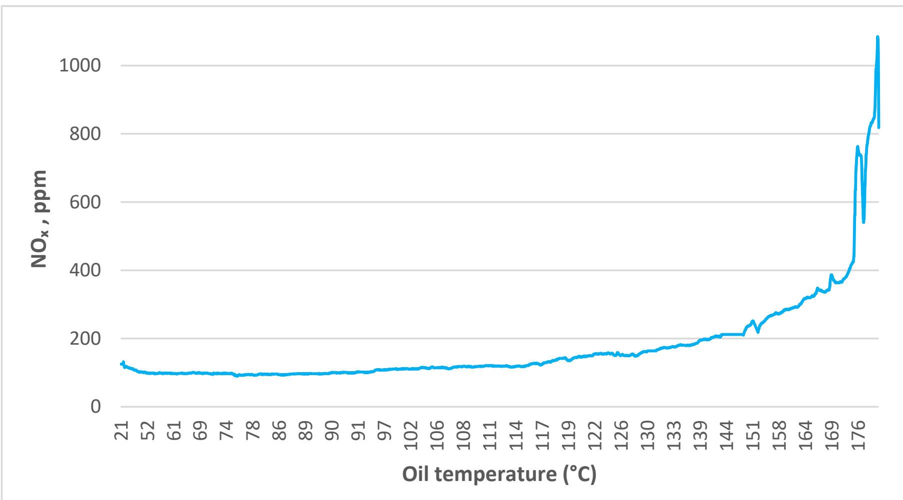

Figure 19. Nitrogen oxides (NO_x) concentration as a function of engine oil temperature.

Overall, the combined analysis of O_2 and NO_x confirms that the change in these components in the exhaust gases during the experiment is determined by progressive thermal loading of the engine, and not by changes in the composition of the fuel–air mixture, which indicates the significant role of temperature escalation as a key factor in the nature of the emission change under idling conditions without forced cooling.

3.3.3. Evolution of Particle Number (PN)

Figure 20 presents the variation in particle number concentration (PNC) as a function of engine oil temperature over the period of the idling experiment without forced cooling. The oil temperature is used as a reference variable to relate the particle emissions to the cumulative thermal state of the engine.

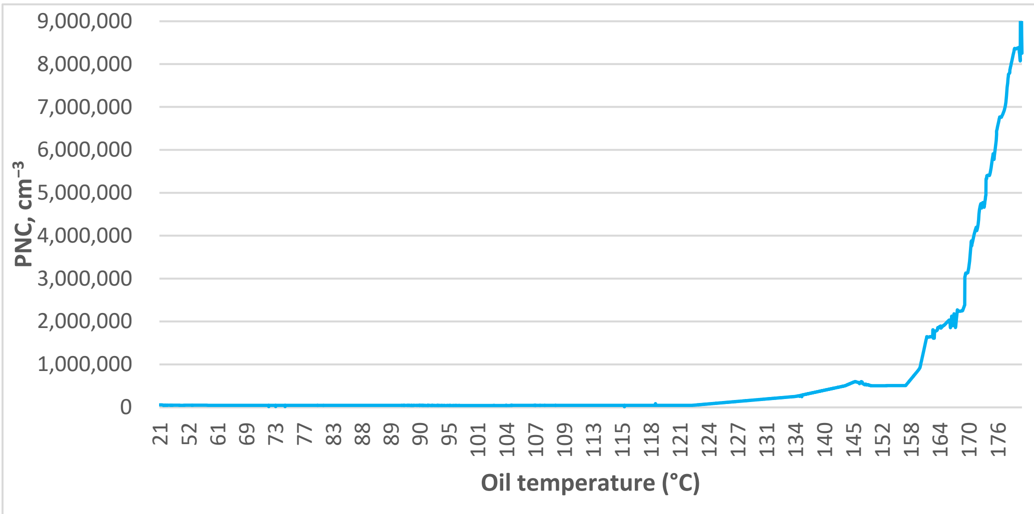

Figure 20. Particle number concentration as a function of engine oil temperature.

At low oil temperatures, up to approximately 120 °C, PN concentrations remain low, with values fluctuating between 4.1×10^4 and 4.5×10^4 cm^{-3}, defining a stable baseline particulate regime under nominal idling conditions.

As the oil temperature increases above 122 °C, PN concentrations gradually rise, reaching approximately 5.4×10^5 cm^{-3} at 149 °C, corresponding to an increase of roughly one order of magnitude relative to the low-temperature baseline.

A distinct transition occurs above 156 °C. Within an oil temperature interval of approximately 156–175 °C, the PN concentration increases from approximately 5.0×10^5 cm^{-3} to peak values in the range of 10^6–10^7 cm^{-3}, corresponding to an additional increase of approximately 1–2 orders of magnitude.

The escalation occurs within a relatively narrow oil temperature window of approximately 20 °C, indicating a threshold-like transition from gradual particulate increase to thermally dominated particle release preceding mechanical blockage.

4. Discussion

The present study provides case-specific experimental evidence for the progressive transition from normal idling to a thermally unstable regime in a high-mileage gasoline engine operating without forced cooling. The results allow a consistent interpretation of the emission behavior under cumulative thermal load in this particular experimental configuration.

https://doi.org/10.3390/en19051137

4.1. Thermal State as a Main Driver of Emission Evolution

The observed emission trends provide an experimental basis for discussing the role of cumulative thermal stress and system-level instability in the investigated engine operating under compromised cooling conditions. The relative stability of oxygen concentration throughout most of the experiment confirms that the stoichiometric fuel–air mixture is not disturbed despite the continuous increase in thermal load. This observation is crucial because it rules out mixture-related effects as the dominant cause of the observed changes in exhaust emission concentrations during internal combustion engine operation. Instead, the changes in CO, HC, NO_x, and PN are primarily driven by the progressive deterioration of thermal conditions during engine operation. On the other hand, the changes in CO_2 values correspond unambiguously to the changes in CO, and may be due to the working oxidation function of the catalytic converter, which fulfills its purpose, regardless of the high and long mileage of the car and the old operating fluids used in the experiment.

The increase in oil temperature, combined with the acceleration of surface-temperature gradients observed in infrared measurements, indicates a gradual departure from thermal equilibrium prior to mechanical failure in the investigated case.

4.2. Interpretation of the Behavior of Gas Emissions Under Thermal Load

The combined analysis of the changes in the components CO, HC, NO_x, and O_2 gives a clear connection of the emission formation process to the increase in the thermal load of the engine. While the oxygen concentration remains largely stable, which confirms the almost continuous formation of a stoichiometric fuel–air mixture during the experiment, all other components considered in this study show changes correlated with the increase in engine oil temperature. However, without chemical speciation or detailed combustion diagnostics, these mechanisms should be interpreted cautiously. Increases in the concentrations of CO and HC reflect the progressive loss of oxidation efficiency in the combustion process and the increasing contribution of lubricant-related hydrocarbons, while the formation of NO_x is dominated by thermally driven kinetics, sharply increasing in the high-temperature regime preceding mechanical engine failure. These findings indicate that, under the imposed cooling impairment scenario, emission behavior in the investigated engine was more strongly associated with cumulative thermal loading than with changes in mixture composition or control parameters.

4.3. Particle Number Escalation and Loss of System Stability

Among all the parameters measured, the particle number shows the most pronounced response to increasing oil temperature. The transition from low and stable PN levels to a rapid, multi-step increase occurs within a relatively narrow temperature range. This behavior marks a clear change from particle formation dominated by the normal combustion process to a regime dominated by thermal load processes in a high range. At elevated engine oil temperatures, the sharp increase in PN concentrations also suggests an increasing contribution from lubricant-related sources, including oil film degradation, evaporation, and release of hydrocarbon material from hot surfaces inside the engine. However, in the absence of particle size distribution or compositional analysis, this interpretation remains a plausible hypothesis rather than a confirmed mechanism. The magnitude and rate of PN increase indicate a loss of thermal stability at the system level, rather than a gradual adjustment of combustion conditions. In this context, PN serves as a sensitive indicator of thermal drift at the system level, even at idle with nominally low load.

https://doi.org/10.3390/en19051137

4.4. Consequences for High-Mileage Engines and Idling

The results demonstrate that prolonged idling under reduced cooling capacity can lead to substantial thermal stress and emission deterioration in the tested engine. The observed emission escalation occurred without significant variation in engine speed or air–fuel ratio, highlighting the role of cumulative thermal effects rather than control parameter changes.

These findings should not be interpreted as universally representative of all high-mileage engines but rather as case-specific evidence of the potential consequences of sustained cooling system impairment. From an emissions perspective, the combined increase in HC, NO_x, and particularly PN under extreme thermal conditions indicates the importance of maintaining effective thermal management even during low-load operation.

4.5. Limitations and Future Work

This work is a single-case, full-scale experiment performed on one high-mileage production engine, with one test run conducted until mechanical seizure. Consequently, the findings should be interpreted as case-specific rather than statistically representative. Engine-specific factors such as prior wear state, lubricant condition, and cooling system characteristics may influence the absolute emission levels and transition thresholds observed. Although acoustic measurements and high-resolution thermographic imaging were recorded during the experiment, they are not treated as the main results in this study. Future work will use these datasets to investigate early warning indicators of thermal instability, such as changes in acoustic signatures associated with lubricant degradation and the spatial evolution of hot spots on the engine and in the engine compartment. Specialized analyses of acoustic emissions and infrared spatial temperature fields are expected to provide additional diagnostic tools for early detection of thermal overload in internal combustion engines. Replication of the experiment under controlled conditions and across engines with different wear histories would be necessary to generalize the observed thermal–emission coupling behavior.

5. Conclusions

This experimental study investigates the changes in components of the exhaust emissions composition of a high-mileage gasoline engine operating at idle without forced cooling until mechanical failure. Based on the results obtained for the investigated engine and operating conditions, the following conclusions can be drawn:

1. Progressive thermal loading under impaired cooling resulted in a continuous increase in oil temperature up to approximately 179 °C, at which mechanical blockage occurred;
2. Particle number emissions exhibited the strongest thermal sensitivity, increasing from approximately 4×10^4 cm^{-3} in the stabilized regime to 10^6–10^7 cm^{-3} in the high-temperature regime, corresponding to an overall escalation of approximately three orders of magnitude;
3. The PN escalation occurred within a relatively narrow oil temperature interval of approximately 156–175 °C, indicating a threshold-like transition associated with loss of thermal stability;
4. Nitrogen oxides showed a sustained temperature-dependent increase, while CO remained comparatively stable under near-stoichiometric conditions, suggesting that emission changes were dominated by cumulative thermal stress rather than mixture variation;
5. Oil temperature proved to be an effective integrative indicator of cumulative thermal exposure and provided a consistent reference variable for correlating emission escalation with progressive loss of thermal equilibrium;

6. The imposed cooling impairment scenario demonstrated that prolonged idling under reduced heat-rejection capacity can lead to severe thermal loading and marked emission deterioration in the tested engine, even in the absence of changes in engine speed or mixture composition.

The findings provide case-specific experimental evidence of the coupling between cumulative thermal stress and emission behavior under cooling system impairment. They should not be interpreted as statistically representative of broader gasoline engine populations. Replicated studies, including particle size distribution and compositional analysis, are required to confirm the underlying mechanisms of PN escalation.

Author Contributions: Conceptualization, I.D., D.S., E.D., V.H., I.N. (Iliyana Naydenova), K.D. and R.M.; methodology, I.D., D.S., E.D., V.H., I.N. (Ivaylo Nachev), K.D. and R.M.; software, G.M., M.S.-M., H.K., L.L., T.I.V., I.N. (Ivaylo Nachev) and D.A.; validation, I.D., D.S., E.D., V.H., I.N. (Iliyana Naydenova), K.D., R.M., G.M., M.S.-M., H.K., L.L., T.I.V., I.N. (Ivaylo Nachev) and D.A.; formal analysis, I.D., D.S., E.D., V.H., K.D., R.M., G.M., H.K., L.L. and T.I.V.; investigation, I.D., D.S., E.D., R.M., G.M., H.K., L.L. and T.I.V.; resources, I.D., D.S., E.D., V.H., I.N. (Iliyana Naydenova), K.D. and R.M.; data curation, G.M., M.S.-M., H.K., L.L., T.I.V., I.N. (Ivaylo Nachev) and D.A.; writing—original draft preparation, I.D., D.S., K.D. and R.M.; writing—review and editing, G.M., M.S.-M., H.K., L.L., T.I.V., I.N. (Ivaylo Nachev) and D.A.; visualization, G.M., M.S.-M., H.K., L.L., T.I.V., I.N. (Ivaylo Nachev) and D.A.; funding acquisition, I.D., D.S., E.D., V.H., I.N. (Iliyana Naydenova), K.D., R.M., G.M., M.S.-M., H.K., L.L., T.I.V., I.N. (Ivaylo Nachev) and D.A. All authors have read and agreed to the published version of the manuscript.

Funding: This research received no external funding.

Data Availability Statement: The original contributions presented in this study are included in the article. Further inquiries can be directed to the corresponding author.

Acknowledgments: This work has been accomplished with financial support from the European Regional Development Fund within the Operational Programme "Bulgarian national recovery and resilience plan", procedure for direct provision of grants "Establishing of a network of research higher education institutions in Bulgaria", and under Project BG-RRP-2.004-0005 "Improving the research capacity anD quality to achieve intErnAtional recognition and reSilience of TU-Sofia (IDEAS)".

Conflicts of Interest: The authors declare no conflicts of interest.

References

1. Bennett, S. *Medium/Heavy Duty Truck Engines, Fuel & Computerized Management Systems*, 6th ed.; Cengage Learning: Boston, MA, USA, 2020; p. 1184, ISBN 978-0357358542.
2. Lodi, F.; Zare, A.; Arora, P.; Stevanovic, S.; Ristovski, Z.; Brown, R.J.; Bodisco, T. Cold idle vs hot idle: Gaseous and particulate emissions using a third-generation oxygenated biofuel. *Renew. Energy* **2024**, *236*, 121414. [CrossRef]
3. Turabimana, P.; Sohn, J.W.; Choi, S.-B. A Novel Active Cooling System for Internal Combustion Engine Using Shape Memory Alloy Based Thermostat. *Sensors* **2023**, *23*, 3972. [CrossRef] [PubMed]
4. Zhang, J.; Xu, Z.; Lin, J.; Lin, Z.; Wang, J.; Xu, T. Thermal Characteristics Investigation of the Internal Combustion Engine Cooling-Combustion System Using Thermal Boundary Dynamic Coupling Method and Experimental Verification. *Energies* **2018**, *11*, 2127. [CrossRef]
5. Pilicita, J.; Domínguez, J.; Torresano, C.; Salazar, B. Impact of internal combustion engine overheating on lubricating oil degradation. *SCT Proc. Interdiscip. Insights Innov.* **2025**, *3*, 428. [CrossRef]
6. Sánchez-Mendoza, A.S.; Vinueza-Morales, M.; Alcázar-Espinoza, J.A.; Pineda-Silva, G.V.; Aucay-García, I.P. Gasoline Vehicle Emissions at High Altitude: An Exploratory STATIS Study in Guaranda, Ecuador. *Atmosphere* **2025**, *16*, 281. [CrossRef]
7. Ebrinc, A.; Cehreli, Z. *Overheating Investigation on 5-Cylinder Engine*; SAE Technical Paper 2007-01-2570; SAE International: Warrendale, PA, USA, 2007. [CrossRef]
8. Moskovchenko, A.; Svantner, M. Thermographic Data Processing and Feature Extraction Approaches for Machine Learn-ing-Based Defect Detection. *Eng. Proc.* **2023**, *51*, 5. [CrossRef]

9. Garrido, I.; Erazo-Aux, J.; Lagüela, S.; Sfarra, S.; Ibarra-Castanedo, C.; Pivarčiová, E.; Gargiulo, G.; Maldague, X.; Arias, P. Introduction of Deep Learning in Thermographic Monitoring of Cultural Heritage and Improvement by Automatic Thermogram Pre-Processing Algorithms. *Sensors* **2021**, *21*, 750. [CrossRef]
10. Ibrahim, M.E. Nondestructive testing and structural health monitoring of marine composite structures. In *Woodhead Publishing Series in Composites Science and Engineering, Marine Applications of Advanced Fibre-Reinforced Composites*; Woodhead Publishing: Cambridge, UK, 2016. [CrossRef]
11. Vicnesh, J.; Salvi, M.; Hagiwara, Y.; Yee, H.Y.; Mir, H.; Barua, P.D.; Chakraborty, S.; Molinari, F.; Acharya, U.R. Application of Infrared Thermography and Artificial Intelligence in Healthcare: A Systematic Review of Over a Decade (2013–2024). *IEEE Access* **2025**, *13*, 5949–5973. [CrossRef]
12. Bauer, J.; Hoq, N.; Mulcahy, J.; Tofail, S.A.M.; Gulshan, F.; Silien, C.; Podbielska, H.; Akbar, M. Implementation of artificial intelligence and non-contact infrared thermography for prediction and personalized automatic identification of different stages of cellulite. *EPMA J.* **2020**, *11*, 17–29. [CrossRef]
13. Brezov, D.; Hristov, H.; Dimov, D.; Alexiev, K. Predicting the Rectal Temperature of Dairy Cows Using Infrared Thermography and Multimodal Machine Learning. *Appl. Sci.* **2023**, *13*, 11416. [CrossRef]
14. Prasad, R.; Gupta, G.; Agarwal, K.; Garg, M.; Ansari, M. Real-Time Fault Detection in Industrial Machinery Using Thermal Imaging and Machine Learning. *Int. J. Perform. Eng.* **2025**, *21*, 529. [CrossRef]
15. Stępień, Z. Premature Degradation of Lubricating Oil during the Service Life of the Positive-Ignition Engine. *Tribol. Online* **2021**, *16*, 31–37. [CrossRef]
16. Smigins, R.; Amatnieks, K.; Birkavs, A.; Górski, K.; Kryshtopa, S. Studies on Engine Oil Degradation Characteristics in a Field Test with Passenger Cars. *Energies* **2023**, *16*, 7955. [CrossRef]
17. Agocs, A.; Nagy, A.L.; Tabakov, Z.; Perger, J.; Rohde-Brandenburger, J.; Schandl, M.; Besser, C.; Dörr, N. Comprehensive assessment of oil degradation patterns in petrol and diesel engines observed in a field test with passenger cars—Conventional oil analysis and fuel dilution. *Tribol. Int.* **2021**, *161*, 107079. [CrossRef]
18. Khrulev, A.E.; Saraiev, O.V. The Method of Expert Assessment of the Technical Condition of an Automobile Engine After Overheating. *Автомобільний Транспорт* **2021**, *48*, 5–16. [CrossRef]
19. Tseng, W.-K.; Mai, T.-J. The Study of Fuel Consumption for Idling Stop Systems in Different Traffic Conditions. *Eur. J. Appl. Sci. Eng. Technol.* **2025**, *3*, 144–154. [CrossRef]
20. Rakha, H.; Ding, Y. Impact of stops on vehicle fuel consumption and emissions. *J. Transp. Eng.* **2003**, *129*, 23–32. [CrossRef]
21. Kapsiz, M.; Durat, M.; Ficici, F. Friction and wear studies between cylinder liner and piston ring pair using Taguchi design method. *Adv. Eng. Softw.* **2011**, *42*, 595–603. [CrossRef]
22. Calabretta, M.; Cacciatore, D.; Carden, P. Valvetrain Friction—Modeling, Analysis and Measurement of a High Performance Engine Valvetrain System. *SAE Int. J. Engines* **2010**, *03*, 72–84. [CrossRef]
23. Hameed, D.K. Effects of Vehicle Mileage Rate on Engine Oil Properties. *Passer J. Basic Appl. Sci.* **2023**, *5*, 59–64. [CrossRef]
24. Tartakovsky, L.; Baibikov, V.; Veinblat, M.; Popescu, D.; Zvirin, Y.; Gutman, M. Mileage Influence on Conversion Efficiency of Catalytic Converter from In-Use Vehicles. *SAE Int. J. Engines* **2012**, *05*, 1617–1623. [CrossRef]
25. Green, D.; Lewis, R.; Dwyer-Joyce, R. *Wear of Valve Train Components Due to Soot Contaminated Lubricant*; SAE Technical Paper 2006-01-1098; SAE International: Warrendale, PA, USA, 2006. [CrossRef]
26. Crozet, M.; Berthier, Y.; Saulot, A.; Jones, D.; Bou-Saïd, B. Valve-seat components in a diesel engine: A tribological approach to limit wear. *Mech. Ind.* **2021**, *22*, 44. [CrossRef]
27. Qiao, C.P. Thermal Fatigue Cracking Phenomenon in Engine Valve Seat Insert. *J. Fail. Anal. Prev.* **2023**, *23*, 2640–2647. [CrossRef]
28. Adelkhani, A.; Daneshkhah, E. Investigation of Engine Lubrication Oil Quality Using a Support Vector Machine and Electronic Nose. *Machines* **2025**, *13*, 121. [CrossRef]
29. Needelman, W.M.; Madhavan, P.V. *Review of Lubricant Contamination and Diesel Engine Wear*; SAE Technical Paper 881827; SAE International: Warrendale, PA, USA, 1988. [CrossRef]
30. Novikov, A.S.; Yanovskii, L.S.; Ezhov, V.M.; Molokanov, A.A.; Sharanina, K.V. Effect of Lubricating-Oil Foamability on Oil-System Operation in Aviation Gas-Turbine Engines. *Chem. Technol. Fuels Oils* **2017**, *53*, 15–22. [CrossRef]
31. Su, R.; Cao, W.; Jin, Z.; Wang, Y.; Ding, L.; Maqsood, M.; Wang, D. Deterioration Mechanism and Status Prediction of Hydrocarbon Lubricants under High Temperatures and Humid Environments. *Lubricants* **2024**, *12*, 116. [CrossRef]
32. Juárez, R.; Petersen, E.L. An experimental apparatus for the study of high-temperature degradation and solid-deposit formation of lubricants. *Rev. Sci. Instrum.* **2024**, *95*, 015109. [CrossRef] [PubMed]
33. Yin, Z.; Zhang, E.; Hao, J.; Li, G. Experimental research on the effect of accelerated aging conditions on the performance of diesel lubricating oil. *E3S Web Conf.* **2021**, *268*, 01012. [CrossRef]
34. Akbiyik, T.; Kahraman, N.; Taner, T. Investigation of the effect of boron additive to lubricating oil on engine performance, exhaust, and emissions. *Fuel* **2022**, *312*, 122931. [CrossRef]

35. Tashev, A.; Ambarev, K.; Paitakov, N.; Nikolov, V. Experimental Investigation of Economic Parameters, Noise and Exhaust Emissions, and Thermal Behavior of a Spark-Ignition Engine Operating with CNG. In Proceedings of the 2025 10th International Conference on Energy Efficiency and Agricultural Engineering (EE&AE), Stara Zagora, Bulgaria, 5–7 November 2025. [CrossRef]
36. Smith, T.; Kersey, V.; Bidwell, T. *The Effect of Engine Age, Engine Oil Age and Drain Interval on Vehicle Tailpipe Emissions and Fuel Efficiencyp*; SAE Technical Paper 2001-01-3545; SAE International: Warrendale, PA, USA, 2001. [CrossRef]
37. Silva, C.; Costa, M.; Farias, T.; Santos, H. Evaluation of SI engine exhaust gas emissions upstream and downstream of the catalytic converter. *Energy Convers. Manag.* **2006**, *47*, 2811–2828. [CrossRef]
38. Zaloznov, A.; Pevnev, N.; Trofimova, L. Dependences of the warm-up time changes of catalytic converters in the open storage car conditions. *MATEC Web Conf.* **2021**, *341*, 00051. [CrossRef]
39. Seo, J.; Yun, B.; Kim, J.; Shin, M.; Park, S. Development of a cold-start emission model for diesel vehicles using an artificial neural network trained with real-world driving data. *Sci. Total. Environ.* **2022**, *806*, 151347. [CrossRef]
40. Kralov, I.; Nedelchev, K. Lowering the noise level in the transport flows through reduction of the traffic barrier reflected noise. *IOP Conf. Ser. Mater. Sci. Eng.* **2019**, *618*, 012051. [CrossRef]
41. Ning, D.; Hou, J.; Gong, Y.; Zhang, Z.; Sun, C. Auto-identification of engine fault acoustic signal through inverse trigonometric instantaneous frequency analysis. *Adv. Mech. Eng.* **2016**, *8*, 1687814016641840. [CrossRef]
42. Shaymukhametov, R.; Strekalov, V. The Acoustic Spectrums of the Combustion Process in the IC-Engines. *MATEC Web Conf.* **2018**, *209*, 00026. [CrossRef]
43. Karpenko, M.; Ževžikov, P.; Stosiak, M.; Skačkauskas, P.; Borucka, A.; Delembovskyi, M. Vibration Research on Centrifugal Loop Dryer Machines Used in Plastic Recycling Processes. *Machines* **2024**, *12*, 29. [CrossRef]
44. Tuleski, B.L.; Yamaguchi, C.K.; Stefenon, S.F.; Coelho, L.d.S.; Mariani, V.C. Audio-Based Engine Fault Diagnosis with Wavelet, Markov Blanket, ROCKET, and Optimized Machine Learning Classifiers. *Sensors* **2024**, *24*, 7316. [CrossRef] [PubMed]
45. Kaul, B.C.; Lawler, B.; Zahdeh, A. Engine Diagnostics Using Acoustic Emissions Sensors. *SAE Int. J. Engines* **2016**, *09*, 684–692. [CrossRef]
46. Du, C.; Sheng, C.; Liang, X.; Rao, X.; Guo, Z. Effects of Temperature on the Tribological Properties of Cylinder-Liner Piston Ring Lubricated with Different Oils. *Lubricants* **2023**, *11*, 115. [CrossRef]
47. Heredia-Cancino, J.; Ramezani, M.; Álvarez-Ramos, M. Effect of degradation on tribological performance of engine lubricants at elevated temperatures. *Tribol. Int.* **2018**, *124*, 230–237. [CrossRef]
48. Rahmani, R.; Rahnejat, H.; Fitzsimons, B.; Dowson, D. The effect of cylinder liner operating temperature on frictional loss and engine emissions in piston ring conjunction. *Appl. Energy* **2017**, *191*, 568–581. [CrossRef]
49. Klyatis, L. *The Basis of Automotive Engineering Accelerated Testing*; SAE Technical Paper 2024-01-2425; SAE International: Warrendale, PA, USA, 2024. [CrossRef]
50. Wang, S.; Yue, T.; Wang, D.; Wahab, M.A. Effect of wear debris on fretting fatigue crack initiation. *Friction* **2022**, *10*, 927–943. [CrossRef]
51. Takabi, J.; Khonsari, M. On the thermally-induced seizure in bearings: A review. *Tribol. Int.* **2015**, *91*, 118–130. [CrossRef]
52. Yi, H.; Seo, J.; Yu, Y.S.; Lim, Y.; Lee, S.; Lee, J.; Song, H.; Park, S. Effects of lubricant-fuel mixing on particle emissions in a single cylinder direct injection spark ignition engine. *Sci. Rep.* **2022**, *12*, 18. [CrossRef]
53. Guido, C.; Napolitano, P.; Di Domenico, D.; Di Maio, D.; Beatrice, C.; Griffaton, B.; Obrecht, N. Exploiting Lubricant Formulation to Reduce Particle Emissions from Gas Powered Engines. *Energies* **2024**, *17*, 3781. [CrossRef]
54. Catapano, F.; Di Iorio, S.; Magno, A.; Sementa, P.; Vaglieco, B.M. A Complete Assessment of the Emission Performance of an SI Engine Fueled with Methanol, Methane and Hydrogen. *Energies* **2024**, *17*, 1026. [CrossRef]
55. Giechaskiel, B.; Valverde, V.; Kontses, A.; Melas, A.; Martini, G.; Balazs, A.; Andersson, J.; Samaras, Z.; Dilara, P. Particle Number Emissions of a Euro 6d-Temp Gasoline Vehicle under Extreme Temperatures and Driving Conditions. *Catalysts* **2021**, *11*, 607. [CrossRef]
56. Jin, D.; Choi, K.; Myung, C.-L.; Lim, Y.; Lee, J.; Park, S. The impact of various ethanol-gasoline blends on particulates and unregulated gaseous emissions characteristics from a spark ignition direct injection (SIDI) passenger vehicle. *Fuel* **2017**, *209*, 702–712. [CrossRef]
57. Taylor, R.I. Fuel-Lubricant Interactions: Critical Review of Recent Work. *Lubricants* **2021**, *9*, 92. [CrossRef]
58. Apicella, B.; Catapano, F.; Di Iorio, S.; Magno, A.; Russo, C.; Sementa, P.; Tregrossi, A.; Vaglieco, B.M. Impact of fuel and lubricant oil on particulate emissions in direct injection spark ignition engines: A comparative study of methane and hydrogen. *Fuel Process. Technol.* **2024**, *265*, 108144. [CrossRef]
59. Available online: https://www.brainbee.mahle.com/brainbee/en/product-lines/emission/ags-200/index-2.jsp (accessed on 15 January 2025).
60. Available online: https://www.texa.com/products/gasbox2-opabox-autopower/ (accessed on 15 January 2025).

61. Regeling van de Staatssecretaris van Infrastructuur en Waterstaat van 16 juni 2022, nr. IENW/BSK-2022/133898, tot Wijziging van de Regeling Erkenning en Keuringsbevoegdheid APK in Verband met de Invoering van de APK-Roetfiltercontrole Met Deeltjesteller en Een Enkele Andere Wijziging. Available online: https://zoek.officielebekendmakingen.nl/stcrt-2022-16212.html (accessed on 15 January 2025).
62. *PTB-A 12.16*; Requirements for Non-Automatic Weighing Instruments. Physikalisch-Technische Bundesanstalt: Braunschweig, Germany, 2016.
63. Available online: https://www.raythink-tech.com/product/rm200f-handheld-thermal-camera/?compare=2170 (accessed on 15 January 2025).
64. Available online: https://www.mouser.bg/ProductDetail/Pimoroni/PIM366?qs=sGAEpiMZZMuqBwn8WqcFUj2aNd7i9W7ulzTeQCQdqjcj2EguumjjPg== (accessed on 15 January 2025).
65. Available online: https://www.mouser.bg/ProductDetail/Pimoroni/PIM365?qs=sGAEpiMZZMuqBwn8WqcFUj2aNd7i9W7u5ZGkA272%252BljHEioCoZ477A== (accessed on 15 January 2025).